Accepted Manuscript

A low frequency multibeam assessment: Spatial mapping of shallow gas by enhanced penetration and angular response anomaly

J. Schneider von Deimling, W. Weinrebe, Zs. Tóth, H. Fossing, R. Endler, G. Rehder, V. Spieß

PII: S0264-8172(13)00048-2

DOI: 10.1016/j.marpetgeo.2013.02.013

Reference: JMPG 1692

To appear in: *Marine and Petroleum Geology*

Received Date: 11 August 2012

Revised Date: 15 November 2012

Accepted Date: 23 February 2013

Highlights,

The highlights were given in the Cover Letter of the first submission.
This is a revised manuscript submission according to a minor revisions review.

Best regards

Jens Schneider v. D.

A low frequency multibeam assessment: Spatial mapping of shallow gas by enhanced penetration and angular response anomaly

J. Schneider von Deimling[1, 2], W. Weinrebe[1], Zs. Tóth[3], H. Fossing[4], R. Endler[2], G. Rehder[2], V. Spieß[3]

1 Helmholtz Centre for Ocean Research (GEOMAR), Wischhofstr. 1-3, 24148 Kiel, Germany

2 Leibniz Institute for Baltic Sea Research Warnemünde (IOW), Seestr. 15, 18119 Rostock, Germany

3 University Bremen, Department of Geosciences, Klagenfurter Str., 28359 Bremen, Germany

4 Aarhus University, Department of Bioscience, Vejlsøvej 25, DK-8600 Silkeborg, Denmark

Corresponding author: J. Schneider v. Deimling

Dr. Jens Schneider von Deimling

Helmholtz Centre for Ocean Research (GEOMAR), Marine Geodynamics, Wischhofstr. 1-3, 24148 Kiel, Germany

Tel. +49-431-600-2660

Fax +49-431-600-2922

Email: jschneider@geomar.de

Abstract

This study highlights the potential of using a low frequency multibeam echosounder for detection and visualization of shallow gas occurring several meters beneath the seafloor. The presence of shallow gas was verified in the Bornholm Basin, Baltic Sea, at 80 m water depth with standard geochemical core analysis and hydroacoustic subbottom profiling. Successively, this area was surveyed with a 95 kHz and a 12 kHz multibeam echosounder (MBES). The bathymetric measurements with 12 kHz provided depth values systematically deeper by several meters compared to 95 kHz data. This observation was attributed to enhanced penetration of the low frequency signal energy into soft sediments. Consequently, the subbottom geoacoustic properties contributed highly to the measured backscattered signals. Those appeared up to 17 dB higher inside the shallow gas area compared to reference measurements outside and could be clearly linked to the shallow gas front depth down to 5 meter below seafloor. No elevated backscatter was visible in 95 kHz MBES data, which in turn highlights the superior potential of low frequency MBES to image shallow sub-seafloor features. Small gas pockets could be resolved even on the outer swath (up to 65°). Strongly elevated backscattering from gassy areas occurred at large incidence angles and a high gas sensitivity of the MBES is further supported by an angular response analysis presented in this study. We conclude that the MBES together with subbottom profiling can be used as an efficient tool for spatial subbottom mapping in soft sediment environments.

Keywords: multibeam; hydroacoustics; methane; shallow gas; bubbles; backscatter; acoustic penetration; Baltic Sea; angular response

1 Introduction

Methane is considered the most important greenhouse gas on Earth after water vapor and CO_2. Recent studies suggest an even higher impact of CH_4 on global warming (Shindell et al., 2009) compared to earlier assumptions (Lelieveld and Crutzen, 1993). Marine methane has been reported to occur worldwide especially on the continental margins, in estuaries and river deltas, where the gas is often hosted in sediments a few decimeters to meters below the seafloor (Judd and Hovland, 2007). Global warming and eutrophication can accelerate natural seabed gas generation by enhancing organic matter accumulation which upon burial is converted to methane. Gas generation and respective bubble formation have a strong impact on the structural integrity and load-bearing capabilities of the sediment (Briggs and Richardson, 1996). Therefore an understanding of presence and distribution of shallow gas in the sediment is of great importance e.g. with regard to offshore construction safety issues. Best et al. (2006) argued that abnormally high levels of methane gas in seafloor sediments could pose a major hazard to coastal populations within the next 100 years through the impact on climate change and sea level rise.

Indications of shallow gas occurrence in the seafloor can be derived from geochemical analyses in the water column and on sediment cores. Even small amounts of free gas may significantly alter the geoacoustic properties of the seafloor, giving rise to highly enhanced acoustic scattering compared to the surrounding sediment/pore water mixture (Anderson and Hampton, 1980; Lyons et al. 1996). Thus, vessel-operated hydroacoustic subbottom profilers were established as a standard tool for remote sensing of shallow gas (Fleischer et al., 2001).

Today a wide range of multibeam echosounder (MBES) mapping systems is available covering frequencies between 12 kHz and 700 kHz. High frequencies offer high resolution at the cost of higher attenuation and low seafloor penetration. In contrast, low frequency multibeam sounders have lower resolution but allow greater operating ranges and potentially deeper seafloor penetration. Recent developments in hardware and processing have significantly improved MBES data and today additional seafloor information can be derived from backscatter analyses and statistical approaches (Brown et al., 2011; Simons and Snellen, 2009; Preston 2009). Those studies mainly examine high frequency data (~100 kHz) for seafloor classification based on the relation between seafloor roughness and backscattering strength. Fonseca et al. (2002) demonstrated the potential of MBES for shallow gas sensing, however, their 95 kHz signals only allowed for a decimeter penetration into the seafloor.

Early studies performed with the sidescan sonar GLORIA (Mitchell, 1993) demonstrated the potential of low frequency approaches at low grazing angles for sediment investigations. Data in the focus of this study were gathered with a low frequency multibeam echosounder (see description below). Our approach was to make use of an enhanced seafloor penetration of a few meters with this low frequency MBES to promote increased subbottom volume scattering and thus mapping of shallow gas over large areas.

2 Methods

Data were acquired on the German R/V Maria S. Merian (Cruise 16/1) in August 2010. A Kongsberg EM120 (12 kHz, hull-mounted), an EM1002 (95 kHz, moonpool), and an ATLAS PARASOUND DS3 (PS, 4 kHz, hull-mounted) system were connected to a Seapath DGPS positioning and motion reference unit. Keel sound velocity and vertical sound velocity profile data were derived from online thermosalinographic and CTD cast measurements. Both MBES used a 2°x2° TX/RX aperture forming 191 and 111 beams, and covered a 140° and 150° swath, respectively. The pulse length was set shortest (2 ms, 0.2 ms) to achieve a maximum range resolution. Depth below seafloor estimates were performed by multiplication of the subbottom travel time (s) with the value of the deepest sound velocity measurement sampled close to the seabed ($v = 1459\ ms^{-1}$). Corrections accounting for seawater attenuation and geometrical spreading were applied by the recording software SIS. Then average backscattering strength (BS) values were computed by the system for data around the detected depth-time sample in each beam. The recorded soundings were cleaned and gridded using the *MB System* software package. Backscatter data were extracted by *MB System* (raw) and *QPS-IVS Geocoder 7.3* (corrected). The MBES systems were calibrated for roll, pitch, yaw, and latency, but not for absolute echo level voltage measurements. Accordingly all BS data must be regarded as relative values with an accuracy specified by the manufacturer to +-1dB. The data in this paper were acquired at shallow water; thus near-field effects add as an extra uncertainty.

3 Field Site & Survey

The study area is located in the Bornholm Basin – a 90 m deep sedimentary basin in the western part of the Baltic Sea (Figure 1). The basin reflects deeper structures and has been influenced by tectonics during the Cenozoic and Mesozoic. Recently, sediments have been deposited in the late Pleistocene during and after deglaciation. The uppermost layer of several meters thickness consists of organic rich silt (Holocene mud) deposited after the Littorina transgression (Figure 2a, upper layer). Morphology and thickness variation of the muddy unit are strongly controlled by postglacial basin development and bottom current pathways. Within this layer widespread occurrences of shallow gas were observed (Hinz, 1971; Laier and Jensen, 2007, Figure 2 left part). Recent measurements of water column methane concentrations close to the seabed (Schmale et al., 2010) further indicated the presence of significant shallow methane sources in the seabed of this area.

4 Results and Discussion

Six survey lines of approximately 2 nautical miles length were run in the northern part of the Bornholm Basin at 4 knots recording EM120 and PS data in parallel; two survey lines were repeated with the EM1002 MBES. Finally, Rumohr Lot (RL) cores were taken at each of five stations along the transect line and respective CH_4 concentrations were measured onboard.

4.1 Evidence of shallow gas from seismic and geochemical profiling

PS records and Rumohr Lot core data disclosed two regimes, A and B, where Holocene mud appeared with and without free methane gas. To the left in Figure 2a a scattering reflector is interpreted as the upper gas front within the Holocene mud between 1 m and 5 m below sea floor (bsf). Below this depth methane gas bubbles efficiently absorbed the acoustic energy and thus 'blanked' any information from the underlying sedimentary strata. In the middle of the profile (Figure 2a) a transition zone T between A and B is characterized by the down-dipping shallow gas front from 2 m to 5 m bsf. To the right the blanking effect is absent revealing the 12 m thick layer of acoustically transparent Holocene mud followed by well-layered deposits of earlier Baltic Sea stages (Ancylus to late Pleistocene). Five core samples along the recorded PS profile (positions see Figure 2a) support the findings from the seismic records, i.e. the measured methane concentration gradients in 1 m long RL cores are high in A and low in B. Sampling procedures for dissolved methane in pore waters were optimized to minimize gas loss even when concentrations exceed solubility at 1 atm (Figure 2b) by drilling into the core liner and immediate sampling. Loss of gas from the base of the core is evident at the gas-rich core c31 (Figure 2b). From core c31 the free gas depth is estimated to be around 0.9 m bsf from Figure 2b by assuming a linear gradient between the sulfate-methane transition zone and the level where gas saturation and consequently free gas occurrence is reached. The horizon of shallow gas occurrence is gradually appearing at greater sediment depth for cores c103, c102, and c101. No free gas is expected from geochemical readings underneath core c32.

Physical property measurements of short core samples (0-0.7 m bsf) reveal very low wet bulk density values of 1040 - 1280 kg m^{-3}, high fractional porosities of 0.96 - 0.82 and sound velocity ratios between sediment and seawater of 0.995 - 0.980 (first number indicate the value at the top, second number the value at the bottom of the core). The steepest gradient of the parameters occurs within the uppermost 10 cm of the muddy deposits. All parameters are highly correlated and controlled by the high content of organic carbon, which is indicated by an ignition loss of 22 % - 15 %. Both sound velocity and wet bulk density of the uppermost mud are very close to the corresponding parameters of the overlying sea water resulting in an acoustic transmission coefficient close to 1 with high acoustic energy transfer into the sea bottom. The sound velocity of the uppermost mud is slightly lower than the water sound velocity. Therefore sound waves are refracted towards the vertical at the water seabed interface and there is no critical angle. This phenomenon is not only restricted to the Baltic Sea but also applies for silty clay deep-sea sediments (Hamilton 1974).

4.2 Assessing the shallow gas front in 2D

Two multibeam surveys at 12 kHz and 95 kHz were performed around the echosounder profile P1 shown in Figure 2a. Figure 3a presents the backscatter amplitude draped onto the respective bathymetric grid of the 12 kHz and 95 kHz surveys. The 95 kHz data reveal no alongtrack changes in backscatter and a featureless and flat topography in the range between

78.0 m in the NE and 77.6 m in the SW. The depth of the 95 kHz data exactly matches the visually determined seafloor reflector in the subbottom data (e.g. Figure 2a). Compared to the high frequency data the depth values of the 12 kHz system systematically appear 1-5 m deeper in the Southwest, and up to 12 m deeper in the Northeast. A closer inspection of Figures 3a and 3b reveals that the bottom detector “misinterprets” the 12 kHz signals backscattered from the top of the shallow gas front and the ones backscattered from the base of the Holocene mud as seafloor echoes. With the low-frequency MBES system the significant bottom misdetection was even observed with sonar settings optimized for shallow water seafloor detection and on the outermost parts of the swath, making it possible to resolve small gas pockets (Figure 3a, right side). A correlation between 3170 depth values of the shallow gas front depth and the Holocene base (identified with the PS data, Figure 2) and the depth difference between the 95 kHz and 12 kHz grids reveals a very clear linear correlation (R^2 = 0.93). Thus, the bathymetric grid in Figure 3a presents the spatial distribution of the shallow gas front in the Southwest and the base of the Holocene mud in the Northeast, and in neither case the seafloor. Those artifacts are fostered by the sedimentological properties with low seafloor backscatter, low attenuation of the underlying mud, and high scattering from gas bubbles and the base of the Holocene mud.

The backscatter data generally mimic the bathymetric artifacts. In contrast to the uniform 95 kHz backscatter record, the 12 kHz backscatter image shows a severe alongtrack change of backscattering strength across the transition zone. The shallower the gas front depth is located the higher the subbottom amplitude values get, reaching up to -15dB (Figure 3, left side). This spatial correlation is attributed to an increasing acoustic attenuation with increasing sediment thickness above the shallow gas front. Jackson and Richardson (2007) estimated an attenuation coefficient of 0.1-0.2 dB m^{-1} kHz^{-1} for Holocene mud in the Baltic Sea. The MBES' time varying gain only corrects for a two-way travel attenuation in seawater, being orders of magnitude lower than for mud. Accordingly, for a 2 m bsf deep buried scatterer and attenuation coefficients between 0.1 and 0.2, the recorded backscatter levels from the 12 kHz MBES are considered to be ~ 4-9 dB too low due to the uncompensated attenuation from the overlying sediments.

Very high backscattering strength values have also been observed by Lyons et al. (1996) for gas bearing Holocene mud in the Western Baltic Sea with BS values between -10 and -20 dB for a 15 kHz normal incidence signal. Given the clear relation between the high MBES backscatter together with the existence of shallow gas occurring in subbottom records we attribute the alongtrack backscatter anomalies to enhanced scattering from gas bubbles in the seabed. It should be noted that only relative dB values can be determined, and uncertainties may derive particularly from near-field effects and uncertain amount of attenuation.

Recent investigations in the Baltic Sea had shown a close relationship between the depth of the shallow gas front and the vertical methane flux within the sediment (Dale et al., 2009). Thus, with this approach and under certain circumstances we foresee low frequency multibeam echo-sounding as a promising, dependable and above all fast spatial mapping tool for shallow gas occurrences in soft sediment.

4.3 Angular response of areas with and without gas

More detailed information about the seafloor can be derived by analyzing the intrinsic behavior of backscatter amplitude over angle via the angular range analysis (Fonseca and Mayer, 2007). While the 95 kHz data reveal normal decay of backscatter strength with angle, significant anomalies appear in the 12 kHz data. Figure 4 shows an averaged angular response plot for 12 kHz raw data (BSr) and those corrected using QPS-IVS *Geocoder 7.3* (Fonseca and Calder, 2005). These corrections account for bathymetric slope and sonar specific parameters such as source level, beam patterns, receiver sensitivity, and time varying gains. It appears that raw and corrected values are very similar, which we attribute to the flat bathymetry.

The angular response outside the gassy regime gives -10 dB at 0° incidence angle and a Lambert like decay towards the outer beams to -35 dB, thus resembling the angular response of soft sediments without gas. Backscatter values gathered within the gassy area reveal virtually no angular changes with a high average backscattering strength around -19 dB - much higher than would be expected from mud. At incident angles greater than 45° the BSc in the gas-prone area even increases. Those findings are confirmed by several angular response analyses (compare Figure 4) in gassy areas at various locations, all showing similar results and have never been reported so far.

Previous modeling of and data about angular behavior of 12 kHz MBES data revealed a noticeable decrease of the backscattering strength amplitude towards outer angles (deMoustier and Alexandrou, 1991). Fonseca et al. (2002) showed for a 95 kHz system angular response from gassy sediments revealing -25 to -27 dB backscattering strength between 30° - 60° with an averaged 5 dB difference for areas with and without shallow gas. In contrast, our 12 kHz data reveal -19 dB between 30° and 60° in the gassy area and 13 dB averaged difference compared to the area without shallow gas. Possible reasons for the much higher response to 12 signals in shallow gas environments might be increased volume backscattering due to bubble resonance phenomena (Anderson and Hampton, 1980) and the fact, that a 12 kHz pulse is 8 times less attenuated in mud without gas bubbles than a 95 kHz pulse. Richardson and Briggs (1996) reported lower surficial compressional wave velocity than seawater (slow reflector) for Holocene mud in the Baltic Sea with total transmission of sound into the seafloor at the angle of "intromission" at low grazing angles (Jackson and Richardson, 2007) – a potential explanation for the higher backscattering towards the outer angle. Additionally, the backscatter might also be significantly biased with an angular behavior linked to ray path length variations inside the sediment layer.

An adaption of the prevailing model for a quantitative inversion of backscatter into gas volume was left as a challenging future task. Fonseca et al. (2002) treated gas bubbles as individual discrete scatterers, where the backscattering strengths of individual bubbles simply sum up. At frequencies around 12 kHz several gas bubbles are expected to occur within one wavelength and thus, multiple scattering effects have to be addressed. Moreover, Fonseca et al. (2002) assumed a fixed size distribution of spherical gas bubbles in his model, which will need further justification from field data.

Overall, in 12 kHz data the amplitude difference in areas with and without gas reached -10 dB at nadir and up to +17 dB towards the outer swath at 65°. As the highest differences in backscattering strength between areas with and without gas were measured at the outermost beams, we attribute highest gas-sensitivity of the MBES to the outer angle stressing the benefits of a swath mapping approach.

5 Recommendations

While the method seems to be particularly applicable in shallow water, 12 kHz multibeam systems are mostly available on deep sea vessels carrying the larger and more expensive transducer arrays. Given the linear behavior of attenuation and frequency, less penetration is expected at higher frequencies for the benefit of smaller transducers. By using a 50 kHz system as a compromise, we expect 3 meter penetration into muddy sediments (according to 12 m for 12 kHz), and such systems can therefore be used as mobile versions on smaller vessels for spatial gas mapping.

Data presented in this study were acquired at 80 m water depth in a very soft sediment environment. Mapping of sub-seabed features with low frequency MBES could also be applied in deeper water, where sediments with low values for acoustic velocity, attenuation and reflection coefficients commonly occur (Hamilton, 1974) fostering acoustic penetration. Due to lower attenuation loss from the bubbles at higher ambient pressure even higher sensitivity for shallow gas is expected in deeper water (Fonseca et al., 2002). However, bathymetric artifacts caused from sub-seabed features presented in this study are expected to be less prominent in deeper water due to acoustic pulse stretching and beam widening with greater ranges both reducing the spatial resolution.

In the meantime, modern MBES allow for recording time series data for all beams and full ranges (water column imaging data). Thus, the recorded backscatter data and the bottom detection can be reviewed during postprocessing, and erroneous seafloor detection may be identified as well as subsurface scattering layers. Together with geologic interpretation of center beam subbottom records we consider the inspection of MBES time series data as promising in regards to future sub-seabed investigations.

6 Conclusion

This study demonstrates that shallow gas down to 5 m bsf can be unambiguously spatially assessed in muddy sediments by use of low frequency multibeam echo-sounding. The 12 kHz data indicate at least 12 m deep penetration into the soft seabed with wrong bottom detection, which we used for subbottom interpretations and spatial mapping of shallow gas. The gas front can be reliably identified across the entire multibeam swath from abrupt depth offsets and distinct backscatter anomalies, which is confirmed by seismo-acoustic subbottom records and geochemical core sampling results. Spatial measurements by high resolution MBES even allow resolving smaller individual gas pockets and potentially other high scattering objects buried in soft sediment. It remains to be investigated how this approach would apply in geological settings with sediments having higher acoustic attenuation.

Backscatter investigations demonstrate a high sensitivity of the 12 kHz MBES with shallow gas mapping. Thus an angular response analysis was performed revealing a unique gas-mediated angular response pattern and increasing gas sensitivity towards the outer swath, a finding which is unprecedented in literature and augmenting the potential of MBES for gas detection and classification in shallow water.

7 Acknowledgements

The research leading to these results has received funding from the European Community's Seventh Framework Programme (FP/2007-2013) under grant agreement n° 217246 and n° 03F0488C made with the joint Baltic Sea research and development programme BONUS. Further research contributing to this paper was funded by the German Ministry of Education and Research through grants n° 03G0819A (SUGAR II).

References

Anderson, A. L., L. D. Hampton (1980), Acoustics of gas-bearing sediments I . Background J. Acoust. Soc. Am., 67, 1865-1889, doi:10.1121/1.384453

Best, A.I., M. D. Richardson, B. P. Boudreau, A. G. Judd, I. Leifer, A. P. Lyons, C. S. Martens, D. L Orange, S. J. Wheeler (2006), Shallow seabed methane gas could pose coastal hazard, Eos (2010), 87(22), 213-220 doi:10.1029/2006EO220001

Briggs, K. B., and M. D. Richardson (1996), Variability in in situ shear strength of gassy muds, Geo-Marine Letters, 16(3), 189-195, doi:10.1007/BF01204508.

Brown, C. J., S. J. Smith, P. Lawton, and J. T. Anderson (2011), Benthic habitat mapping: A review of progress towards improved understanding of the spatial ecology of the seafloor using acoustic techniques, Estuarine, Coastal and Shelf Science, 92(3), 502-520.

Dale A. W., P. Regnier, P. Van Cappellen, H. Fossing, J.B. Jensen, B.B Jørgensen (2009), Remote quantification of methane fluxes in gassy marine sediments through seismic survey. Geology, 37(3) 235-238 doi: 10.1130/G25323A.1

deMoustier, C., and D. Alexandrou (1991), Angular dependence of 12- kHz seafloor acoustic backscatter, J. Acoust. Soc. Am., 90(1), 522-531.

Fleischer, P., Orsi, T. H., Richardson, M. D., Anderson, A. L. (2001), Distribution of free gas in marine sediments: a global overview. Geo-Marine Letters, 21(2), 103-122.

Fonseca, L., L. Mayer, D. Orange, N. Driscoll (2002), The high-frequency backscattering angular response of gassy sediments: model/data comparison from the Eel River Margin, California, J. Acoust. Soc. Am, 111(6), 2621-2631, doi:10.1121/1.1471911.

Fonseca L and B. Calder (2005), Geocoder: an efficient backscatter map constructor. In: Proceedings of the U.S. Hydrographic Conference, San Diego, CA.

Fonseca, L., and L. Mayer (2007), Remote estimation of surficial seafloor properties through the application Angular Range Analysis to multibeam sonar data, Marine Geophysical Research, 28, *2*, 119-126.

Hamilton (1974), Prediction of deep-sea sediment properties: State of the art, In: Deep-Sea Sediments, Physical and Mechanical Properties Edt: A.L. Inderbitzen, Plenum Press.

Hinz, K., F. Kögler, I. Richter, E. Seibold (1973), Reflexionsseismische Untersuchungen mit einer pneumatischen Schallquelle und einem Sedimentecholot in der westlichen Ostsee. Teil II Untersuchungsergebnisse und geologische Deutung, Meyniana, 21, 17-24.

Jackson, R. D., M. D. Richardson, (2007), High-Frequency Seafloor Acoustics, Springer, DOI: 10.1121/1.2782933.

Judd, A.G., M. Hovland, (2007), Seabed Fluid Flow Environment, Cambridge University Press. New York doi: 10.2277/ 0521819504.

Laier, T., J. B. Jensen (2007), Shallow gas depth-contour map of the Skagerrak-western Baltic Sea region, Geo-Marine Letters, 27(2) 127-141 doi: 10.1007/s00367-007-0066-2.

Lelieveld, J., P. Crutzen, C. Bruhl (1993), Climate effects of atmospheric methane, Chemosphere, 26(1-4) 739-768 doi: 10.1016/0045-6535(93)90458-H.

Lyons, A. P., M. E. Duncan, A. L. Anderson, J. A. Hawkins (1996), Predictions of the acoustic scattering response of free-methane bubbles in muddy sediments, J. Acoust. Soc. Am., 99(1) 163-172, doi:10.1121/1.414500.

Mitchell, N. C., (1993), A Model for Attenuation of Backscatter due to Sediment Accumulations and Its Application to Determine Sediment Thicknesses With GLORIA Sidescan Sonar, Journal of Geophysical Research, 98, B12, 22.477-22.493, doi:10.1029/93JB02217.

Preston, J. (2009), Automated acoustic seabed classification of multibeam images of Stanton Banks, Applied Acoustics, 70(10), 1277-1287.

Richardson, M.D. and K.B. Briggs, In situ and laboratory geoacoustic measurements in soft mud and hard-packed sand sediments: Implications for high-frequency acoustic propagation and scattering, Geo-Marine Letters, 16, 196-203.

Schmale, O., J. Schneider von Deimling., W. Gülzow, G. Nausch, J, J. Waniek, G. Rehder (2010), Distribution of methane in the water column of the Baltic Sea, Geophysical Research Letters, 37(L12604), 1-5 doi: 10.1029/2010GL043115.

Shindell, D.T., G. Faluvegi, D. M. Koch, G. A. Schmidt, N. Unger, S. E. Bauer (2009), Improved attribution of climate forcing to emissions, Science, 326 716-718, doi:10.1126/science.1174760.

Simons, D. G., M. Snellen (2009), A Bayesian approach to seafloor classification using multi-beam echo-sounder backscatter data, Applied Acoustics, 70(10) 1258-1268 doi:10.1016/j.apacoust.2008.07.013.

Figure Captions

Figure 1: Shallow gas distribution map modified after Laier and Jensen (2007). The working area plots within an area hosting shallow gas within 2-4 m bsf.

Figure 2: Presentation of a transition zone in Holocene mud between areas with and without shallow methane gas (**a**) PS subbottom profile P1 starting with the seafloor at 78 m water depth. A zone with shallow gas occurs to the left (A, red) and is followed by the transition zone (T, green). To the right no shallow gas is present and the Holocene base appears beneath the mud (B, blue). Colored vertical bars mark the position of sediment sampling (Station c31 and c32 are outside of the seismo-acoustic picture, see Figure 3 for location). (**b**) CH_4 concentration depth profile measured for five cores. Methane concentrations were linearly extrapolated to estimate the depth of methane saturation in the seabed at the intersection with the in situ saturation concentration (16.6 mM, yellow line). Also indicated is the solubility relative to a methane gas pressure of 1 atm (black line).

Figure 3: (**a**) Backscatter chart of EM120 (12 kHz, colored) and 95 kHz (grey, transparent) both draped onto their respective bathymetric grids. Strong variations in backscatter and bathymetry occur in the 12 kHz data with high backscattering strength values (BS) to the left (red, gas) and low ones (blue, no gas) to the right part of the figure. This corresponds to the underlying subbottom findings visible in the vertical curtain image (with depth offset for better visibility). The 95 kHz data (grey surface) plots on top of the 12 kHz surface and shows neither amplitude nor bathymetric changes across- or alongtrack (**b**) Depth profiles D1 and

D2 gathered from 12 kHz and 95 kHz bathymetric grids. Depth differences of up to 12 m occur between both data (for location see (a)).

Figure 4: Angular response/range analysis (ARA) for 30 pings showing very distinct differences between backscattering strength (BS) over incidence angle behavior for data gathered within (A, red) and outside of the shallow gas regime (B, blue). BSr (raw) denote uncorrected backscatter values, whereas BSc values were generated with corrections for bathymetric slope and beam patterns realized through GEOCODER. See Figure 3 for exact location.

Figure 1
Click here to download high resolution image

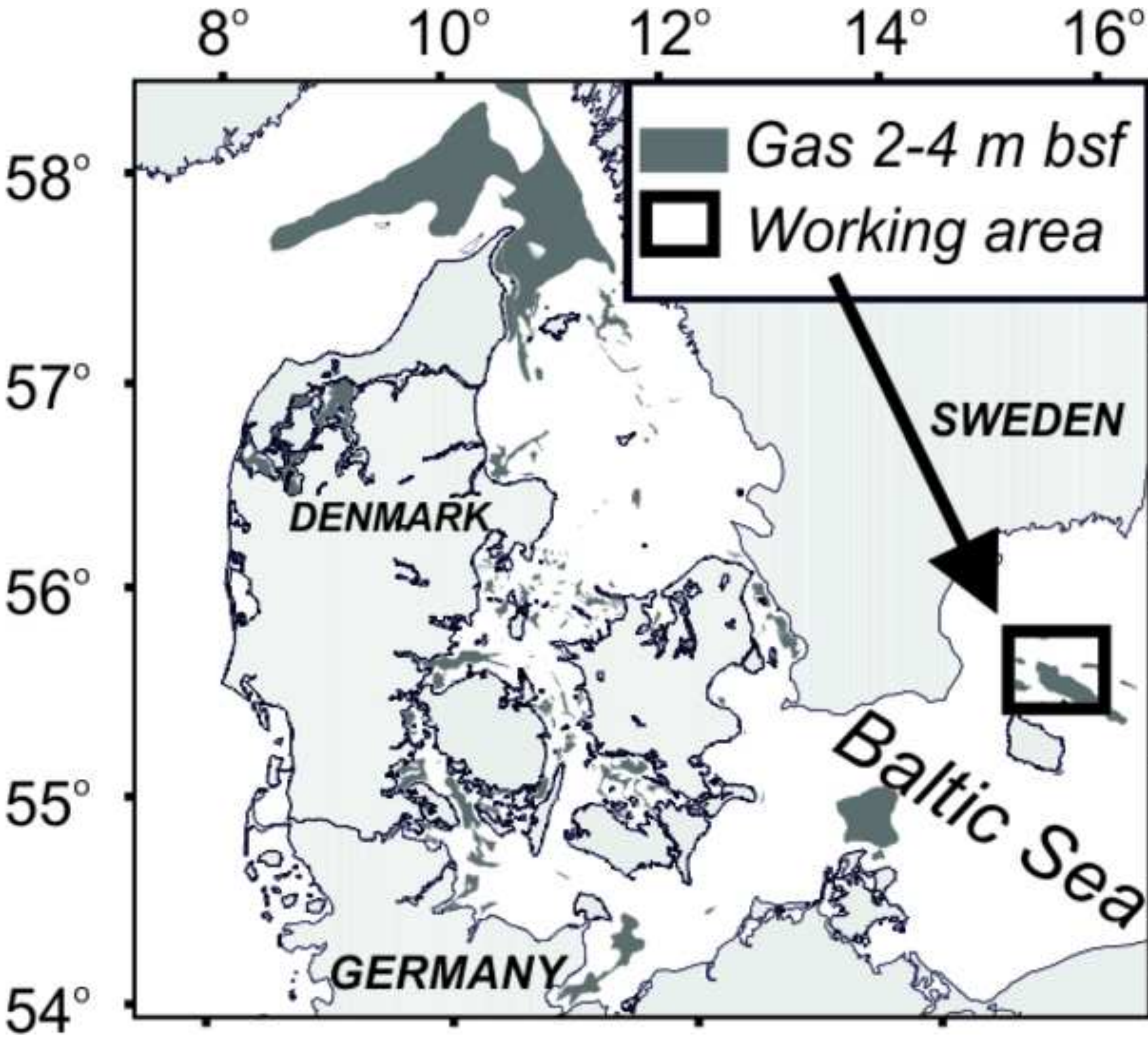

Figure 2
Click here to download high resolution image

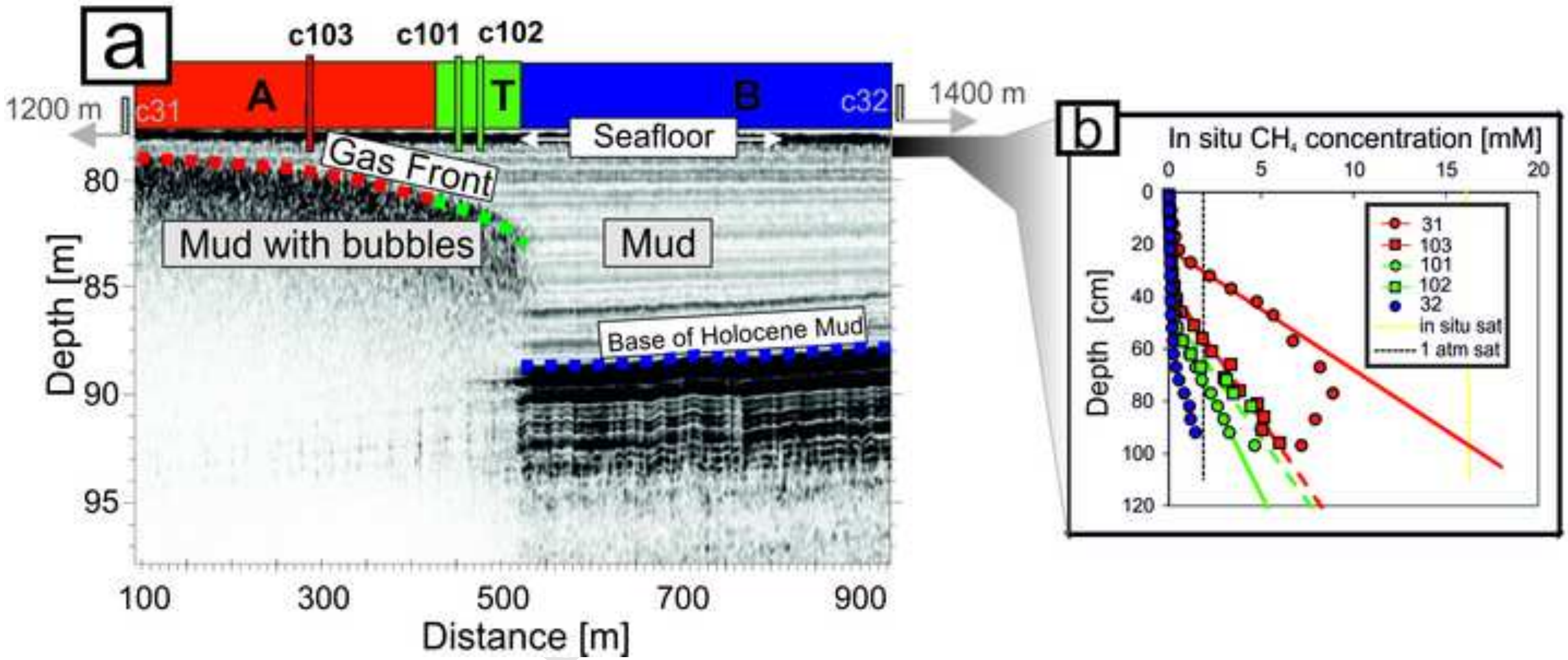

Figure 3
Click here to download high resolution image

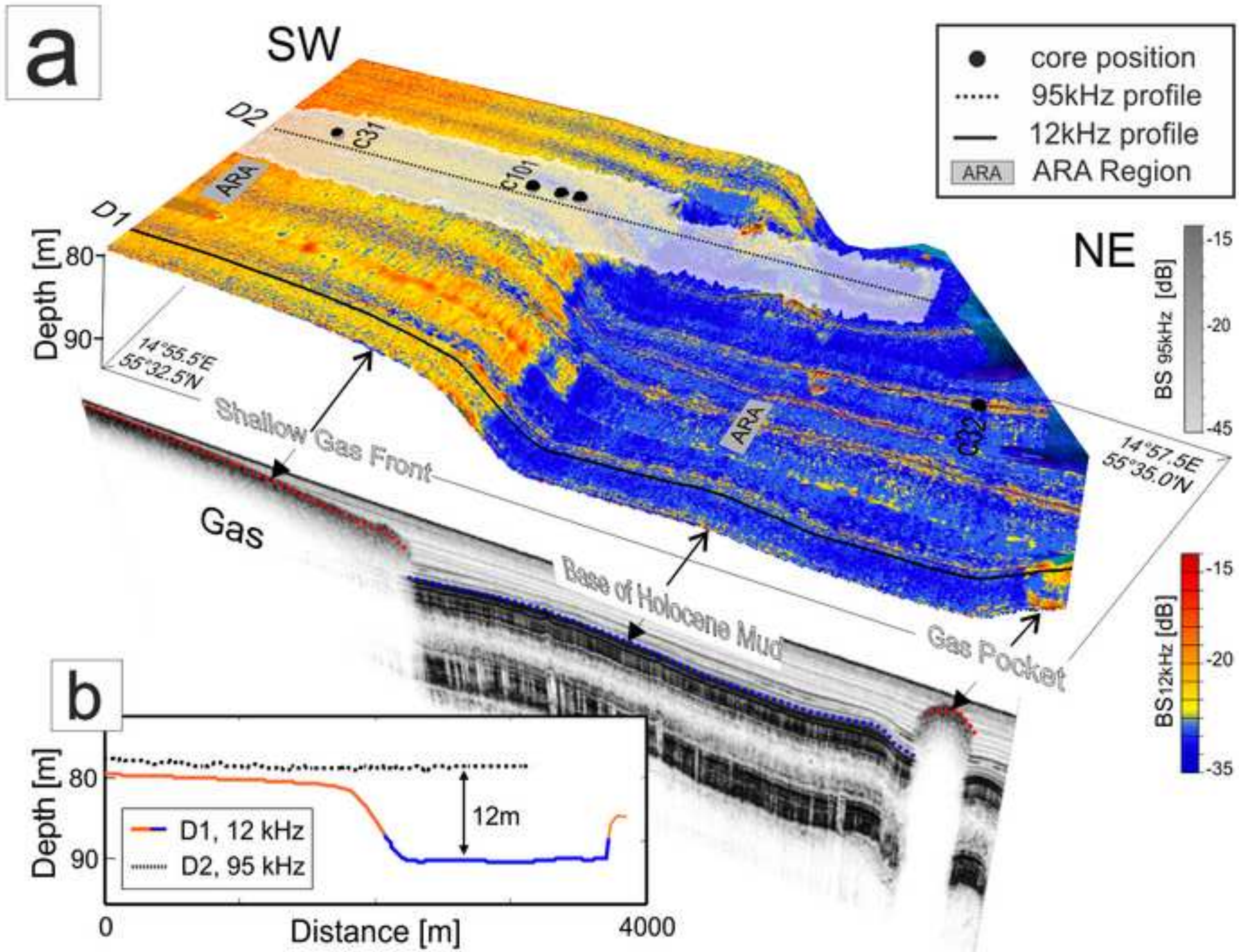

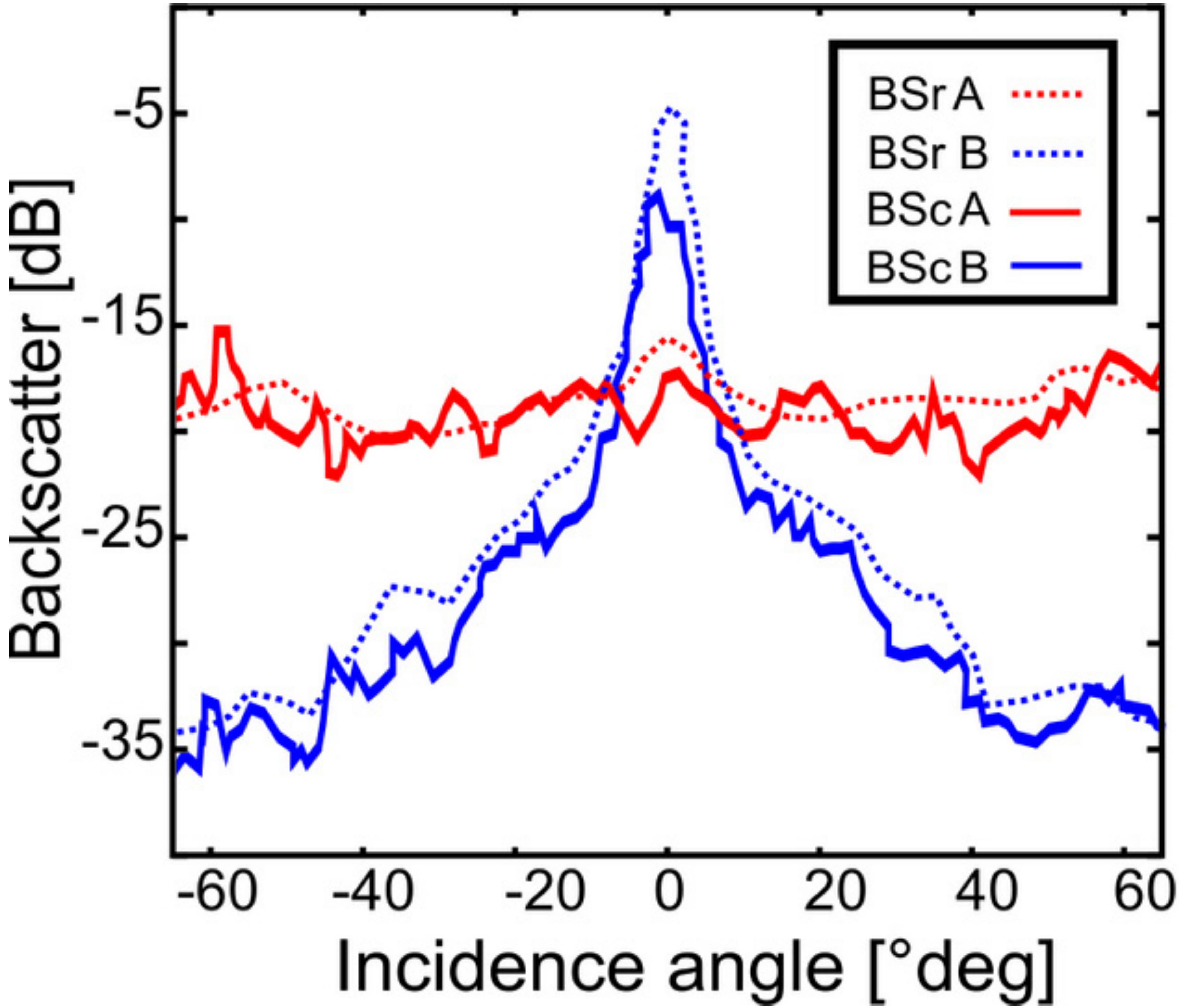
BSr A
BSr B
BSc A
BSc B
-5
-15
-25
-35
Backscatter [dB]
-60
-40
-20
0
20
40
60
Incidence angle [°deg]